applied sciences

MDPI

Article

Dispersion Properties of an Elliptical Patch with Cross-Shaped Aperture for Synchronized Propagation of Transverse Magnetic and Electric Surface Waves

Amagoia Tellechea [1,*], Iñigo Ederra [1,2], Ramón Gonzalo [1,2] and Juan Carlos Iriarte [1,2]

[1] Campus Arrosadía, Public University of Navarra, 31006 Pamplona, Navarra, Spain; inigo.ederra@unavarra.es (I.E.); ramon@unavarra.es (R.G.); jcarlos.iriarte@unavarra.es (J.C.I.)
[2] Campus Arrosadía, Institute of Smart Cities, 31006 Pamplona, Navarra, Spain
* Correspondence: amagoia.tellechea@unavarra.es; Tel.: +34-948-166044

Received: 28 February 2018; Accepted: 16 March 2018; Published: 19 March 2018

Abstract: This paper presents a novel pixel geometry for the implementation of metasurfaces requiring synchronized phase propagation of transverse magnetic (TM) and transverse electric (TE) modes. The pixel is composed by an elliptical metallic patch with an asymmetric cross-shaped aperture in the center, printed on a grounded slab. A practical implementation of a metasurface was carried out employing such a pixel geometry. Simulation results show similar frequency dispersion properties for both modes within the working frequency band, in agreement with the theoretical basis.

Keywords: metasurfaces (MTSs); transverse magnetic (TM); transverse electric (TE); surface waves (SWs); dispersion

1. Introduction

Metasurfaces (MTSs) are composed of a dense layer of subwavelength metallic elements, also called pixels [1–3], printed on top of a grounded substrate. Bounded slow surface waves (SWs) can be guided on these structures with engineered dispersion properties. This is the case for the near-field plates, planar lenses and cloaking structures found in the literature [4–7]. Based on the transverse resonance condition, such structures have been characterized by means of scalar or tensor surface impedances [1]. In general, scalar impedance surfaces can support the propagation of either TM or TE SWs. For simplicity, efforts have been focused on guiding of the single TM mode. In fact, several studies have been carried out to analytically characterize the dispersion properties of the TM mode within circular, elliptical and slotted patches printed on top of a grounded slab [8–12].

However, one of the most interesting application of MTS-based structures is the realization of low-profile lightweight antennas for space applications [13–18]. By modulating the characteristic surface impedance, a transition from a cylindrical SW excited form the center to a leaky-wave (LW) is obtained using a MTS-based structure. By means of the modulation of the scalar or tensor impedance characteristics of the isotropic or anisotropic surfaces, beam pointing, shape and radiated field polarization can be tailored for different applications [13–18]. Most of the configurations found in the literature work in single-mode operation. In fact, a single TM SW is supported in such structures, and consequently, single circular polarization (CP) performance is obtained. In order to obtain dual circularly polarized broadside radiation, two modes of TM and TE nature need to be supported by the MTS [19,20]. In these solutions, both modes must have decoupled propagation, be balanced in amplitude and phase synchronized. When these modes interact with a properly modulated surface impedance tensor, a LW radiates outside the structure towards the broadside with the right-hand (RH) or left-hand (LH) CP, depending on the feed phase. The main goal of this work is to discuss a

practical pixel geometry supporting the propagation of TM and TE modes balanced in phase that can be employed to implement dual circularly polarized MTS antennas.

The paper is structured as follows. The theoretical principle for phase-matched dual-mode operation is summarized in Section 2. A pixel geometry that meets this condition is presented in Section 3, where a full-wavefrequency and spatial-dispersion analysis is carried out. Additionally, a phase-balanced single-layer guiding MTS is implemented with these pixels. In Section 4, the simulation results are shown. Finally, conclusions are drawn in Section 5.

2. Theoretical Principle

As it is well known [4–17], guiding metasurfaces (MTSs) support the propagation of surface waves (SWs) characterized by a phase velocity ($v = \omega/\beta$) lower than the free space velocity ($c = \omega/k_0$). Thus, the phase constant of the SWs (β) is larger than the free space wavenumber (k_0): $v < c \rightarrow \beta > k_0$. When a cylindrically symmetric MTS is in the xy plane and these modes are excited from the center of the structure, they propagate in a radial direction, bounded to the surface, following $e^{-j\beta\rho}$ (with $\hat{\boldsymbol{\rho}}$ being the radial unit vector). Away from the structure, the field is evanescent, and it is defined by an exponential decay $e^{-jk_{zo}z}$, fulfilling: $k_0^2 = \beta^2 + {k_{zo}}^2$, where $\Im(k_{zo}) = -\alpha_{zo}$, $\alpha_{zo} > 0$.

The goal of this work is to implement a single-layer metasurface that supports the propagation of a transverse magnetic mode (TM) and a transverse electric mode (TE). As has been widely explained in [8–13], a single-layer MTS can be analyzed in terms of its equivalent circuit model. According to the transverse resonance equation, the surface impedance relating the fields of each SW in the surface ($\boldsymbol{Z_{surf,i}}$) can be related to the free space impedance of each mode at the air-surface interface ($\boldsymbol{Z_{0,i}}$) as: $\boldsymbol{Z_{0,i\ i=TM,TE}} = -\boldsymbol{Z_{surf,i\ i=TM,TE}}$. Thus, the surface impedance of each mode can be described by the following expressions:

$$\boldsymbol{Z_{surf,TM}} = j\,\boldsymbol{X_{surf,TM}} = -\xi\frac{k_{zo}}{\beta} \tag{1}$$

$$\boldsymbol{Z_{surf,TE}} = j\,\boldsymbol{X_{surf,TE}} = -\xi\frac{\beta}{k_{zo}} \tag{2}$$

where $\xi = 120\pi$ is the free space impedance. From Equations (1) and (2), it can be concluded that the surface impedance of the desired MTS must have an inductive reactive term in order to allow the propagation of a TM SW ($X_{surf,TM} > 0$), while the surface impedance must have an inductive reactive term ($X_{surf,TE} < 0$), to support the TE mode propagation.

Both modes must propagate in the structure decoupled and synchronized in phase. The condition for TM and TE modes phase synchronism can also be related to the equivalent surface reactance values as:

$$\boldsymbol{\beta_{TM}} = \boldsymbol{\beta_{TE}} \rightarrow \boldsymbol{X_{surf,TM}}\,\boldsymbol{X_{surf,TE}} = -\xi^2 \tag{3}$$

Exciting the rotationally symmetric MTS from the center by a magnetic dipole (slot in the ground plane in a practical implementation) the TM and TE modes propagate radially from the center. In the MTS configuration shown in Figure 1, the magnetic dipole (depicted as a black arrow) is oriented towards the y-axis. In this case, the TM SW is azimuthally excited following a $\cos(\varphi)$ function, while the field related to the TE mode meets a $\sin(\varphi)$ excitation. If the phase synchronism of the modes is ensured all over the surface and the mode amplitudes are equal, the total field on the surface, obtained as the combination of both modes, provides a linearly polarized E_x field:

$$\boldsymbol{E}^{(y)} = \boldsymbol{E_{TM}}^{(y)} + \boldsymbol{E_{TE}}^{(y)} = -\boldsymbol{E_{TM}}^{(y)}\cos(\boldsymbol{\varphi})\hat{\boldsymbol{\rho}} + \boldsymbol{E_{TE}}^{(y)}\sin(\boldsymbol{\varphi})\hat{\boldsymbol{\varphi}} = -\boldsymbol{E_0}\hat{\boldsymbol{x}} \tag{4}$$

where $E_{TM} = E_{TE} = E_0$ for circular polarization.

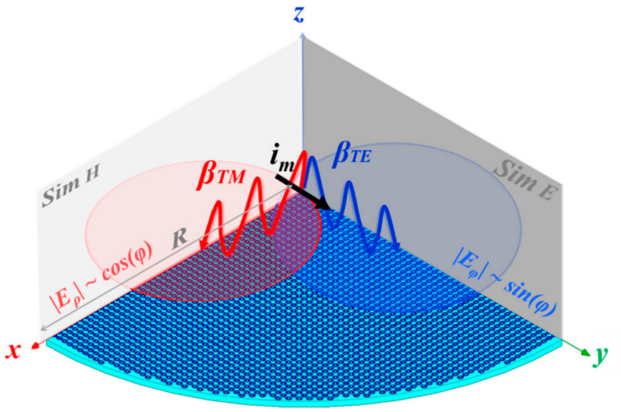

Figure 1. A rotationally symmetric metasurface is excited by a magnetic dipole oriented towards the y-axis: TM and TE SWs propagate radially on the surface phase synchronized. $|E\rho|$ follows a $\cos(\varphi)$ function while $|E\varphi|$ follows a $\sin(\varphi)$ function.

3. Practical Implementation

3.1. Unit Cell Geometry

The geometry of the proposed pixel is shown in Figure 2. An elliptically shaped metallic patch with a cross-shaped aperture is printed on top of a grounded dielectric of AD-1000 material, with a relative permittivity of $\varepsilon_r = 10.2$ and a thickness of $h = 1.27$ mm. The unit cell dimension is $u = 3.14$ mm. The minor axis of the elliptical metallic patch (e_a) is oriented towards the x-axis and the major axis (e_b) towards the y-axis in the rectangular reference system. Inside the metallic patch, there is an asymmetric cross-shaped aperture. The main axes of this cross aperture are also aligned with the rectangular reference, i.e., they are aligned with the ellipse axes. The length and width of the cross are denoted as c_a, w_a and c_b, w_b towards the x and y axis, respectively. Since the main applications of the MTSs composed with such subwavelength elements are in the microwave regime, the metal is treated as a perfect electric conductor, and dielectric losses are neglected.

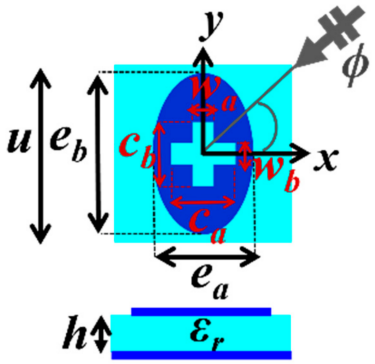

Figure 2. Unit cell geometry composed by a metallic elliptical patch with asymmetric cross-shaped aperture in the center, printed on a grounded substrate. Dimension $u = 3.14$ mm, AD-1000 dielectric with relative permittivity $\varepsilon_r = 10.2$ and thickness $h = 1.27$ mm.

A full wave eigenmode analysis for the supported SWs has been carried out. For this purpose, periodic boundary conditions are imposed in the x and y axis with $k_x u$ and $k_y u$ phasing, respectively. The imposed phasing corresponds to a mode impinging on the cell towards the ϕ angle, which is evanescent in the z direction. Thus, it meets: $k_x{}^2 + k_y{}^2 = \beta_i{}^2 > k_0{}^2$.

3.2. Pixel Dispersion Properties

The transverse magnetic (TM) and transverse electric (TE) modes' spatial and frequency dispersion properties for different patches are shown and compared in this section.

In order to facilitate reader understanding, firstly the TM and TE modes' isofrequency dispersion curves for a pixel composed by an elliptical metallic patch printed on a grounded dielectric (i.e., without cross slot) are shown in Figure 3. The dispersion properties for different elliptical patch ratios (e_a/e_b) are compared.

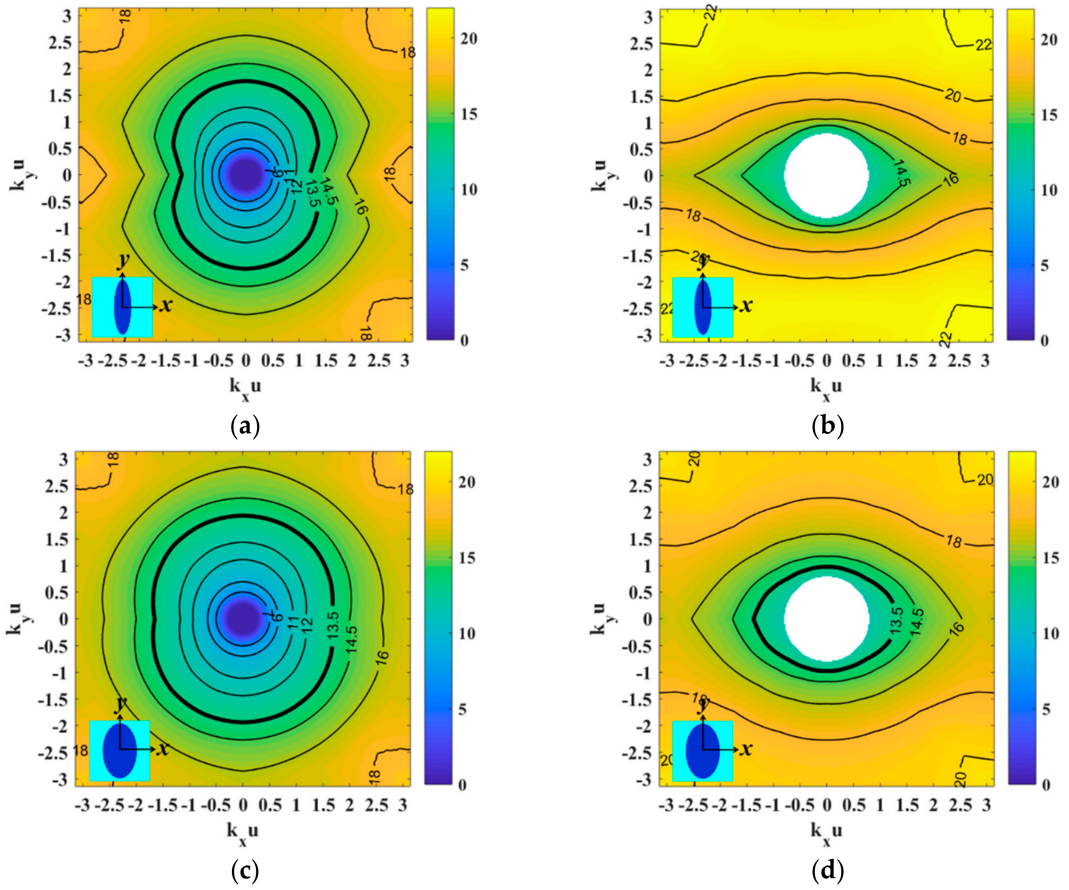

Figure 3. Frequency and spatial dispersion curves for TM (left column) and TE (right column) SWs supported by a pixel composed by a metallic elliptical patch printed on a grounded dielectric with different ratios: (**a**,**b**) e_a/e_b = 0.6 and (**c**,**d**) e_a/e_b = 0.85. The employed dielectric is AD-1000 (ε_r = 10.2, thickness h = 1.27 mm) and the unit cell dimension u = 3.14 mm.

As can be seen in Figure 3a, the phase constant of the supported TM mode (β_{TM}) increases when the electrical size of the patch is larger. The TM phase constant is always larger when the propagation angle is oriented towards the larger axis of the ellipse (in this case the y-axis), and the same effect can be observed in the x-axis when the ratio of the ellipse is increased (Figure 3c). Unlike the TM mode, which is supported in the structure at all frequencies, the TE SW has a cut-off frequency. As can be seen in Figure 3b–d, the cut-off frequency of the TE mode decreases for electrically large patches. For instance, in the patch with larger ellipse ratio (Figure 3d), the TE mode is outside the visible region at 13.5 GHz (shown in bold in the isofrequency curves), while it is inside the visible region for smaller ratios (Figure 3b). The TE phase constant (β_{TE}) increases on the x-axis for ellipses with larger ratios.

When the required MTS must support only the propagation of a TM mode, the geometry and rotations of the selected patches for the MTS implementation must be carefully selected to avoid the propagation of the TE SW working below its cut-off frequency. Nevertheless, in the present work, both

the TM and TE modes must be considered. The main goal is to independently control the propagation properties of both the TM and TE SWs, ensuring, additionally, the synchronized propagation of both modes within a certain impinging angle (ϕ). For this purpose, an asymmetric cross-shaped aperture has been introduced in the center of the previously presented elliptical patch geometry (shown in Figure 2). Frequency and spatial dispersion properties for three geometric parameterizations are shown in Figure 4.

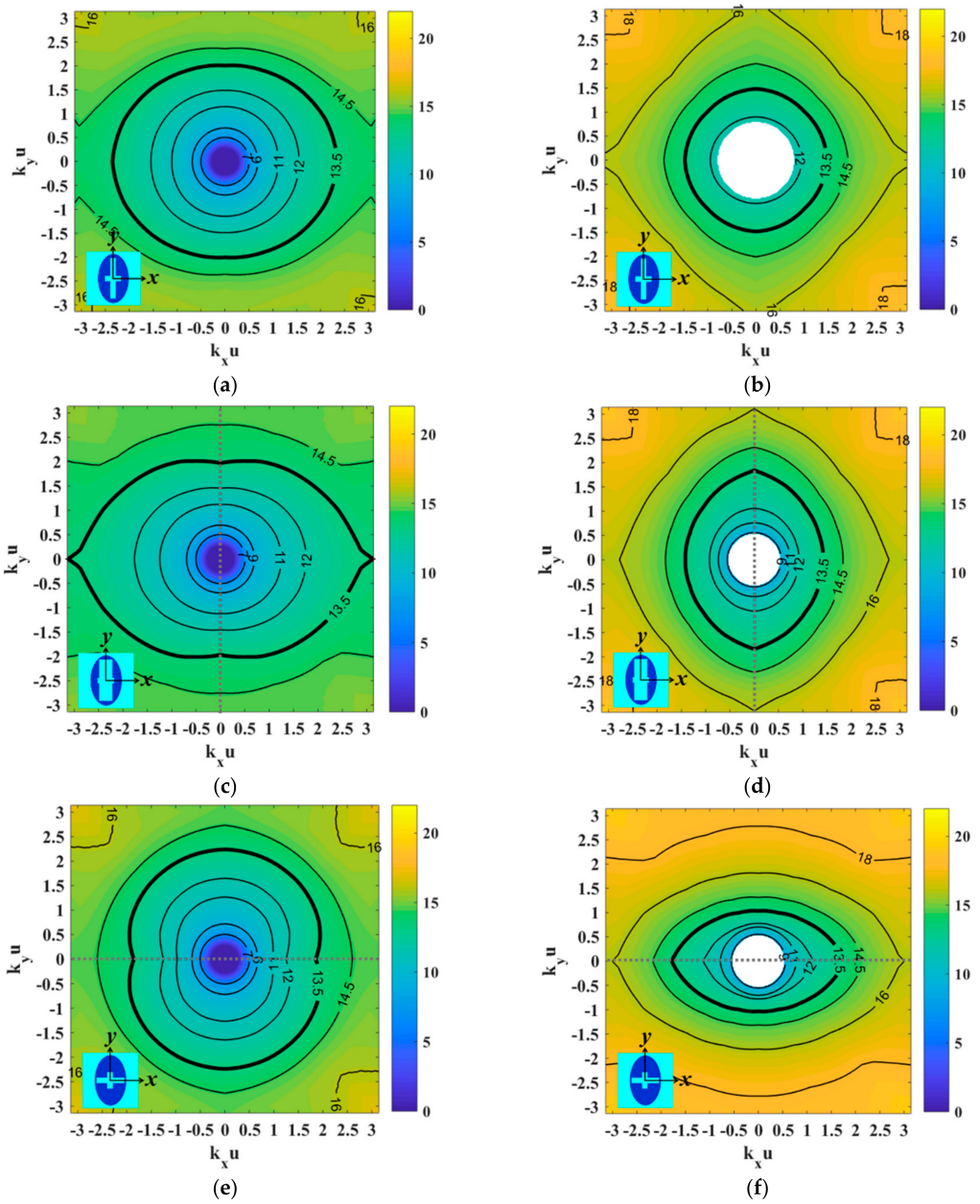

Figure 4. Frequency and spatial dispersion curves for TM (left column) and TE (right column) SWs supported by three different pixels composed by a metallic elliptical patch with an asymmetric aperture in the center, printed on a grounded dielectric. The ellipse ratio for the patches is e_a/e_b = 0.85 in all cases, and cross apertures are defined by (w_a/u, c_a/e_a, w_b/u, c_b/e_b) parameters: (**a**,**b**) pixel A (0.15, 0.6, 0.15, 0.9), (**c**,**d**) pixel B (0.25, 0.6, 0.15, 0.9) and (**e**,**f**) pixel C (0.15, 0.85, 0.15, 0.6). The employed dielectric is AD-1000 (ε_r = 10.2, thickness h = 1.27 mm) and the unit cell dimension u = 3.14 mm.

Given that the unit cell dimension is very small in terms of wavelength, the inclusion of the asymmetric cross-shaped aperture in the center of the elliptical patch geometry makes it possible to control the phase constant of the different modes (β_{TM}, β_{TE}) independently when impinging on the unit cell with different angles. TM mode dispersion properties are affected by the slot of the cross perpendicular to the impinging angle, while the TE SW is affected by the slot aligned with the incidence direction. In Figure 4a, the cross slot along the larger axis of the elliptical patch (y-axis) has been enlarged, increasing the c_b parameter. Due to this fact, when a TM mode propagates in the unit cell along the x-axis, β_{TM} increases considerably. Increasing c_b also affects the dispersion properties of the TE mode (Figure 4b); when the mode propagates in the cell towards $\phi = 90°$, β_{TE} increases in the y-axis. On the other hand, the effect of broadening the slot corresponds to an electrically larger patch. In Figure 4c,d, the slot width towards the x-axis (w_a parameter) is enlarged, and due to this effect, β_{TM} and β_{TE} increase when TM and TE modes propagate in the cell at angle of $\phi = 0°$ and $\phi = 90°$, respectively.

It is necessary to remark that this patch geometry is especially attractive due to the multiple possibilities for its geometrical parameterization, which make it possible to independently control the dispersion properties for both TM and TE modes within a certain frequency band. For instance, the patch geometry shown in Figure 4c,d (pixel B) allows the synchronized propagation of TM and TE SWs when impinging on the patch along its larger axis (in this case, $\phi = 90°$) at 13.5 GHz. As can be seen, the isofrequency curves of both modes coincide at this frequency, and the phase constant of both modes is the same: $\beta_{TM} = \beta_{TE} = 597$ rad/m. However, the modes' synchronization can be also obtained with other geometrical parameterization. This is the case, for instance, for pixel C (shown in Figure 4e,f), in which the cross slot is increased along the shorter axis of the ellipse (c_a parameter has been increased). This geometry also ensures $\beta_{TM} = \beta_{TE} = 597$ rad/m at 13.5 GHz, when TM and TE modes impinge on the cell along the $\phi = 0°$ angle. This feature is also shown in Figure 5.

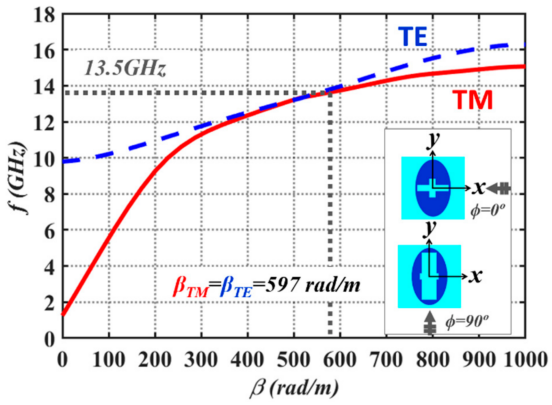

Figure 5. Frequency dispersion properties for TM and TE modes when impinging on pixel B at $\phi = 0°$. Curves agree with the frequency dispersion of the modes for pixel C within $\phi = 90°$ angle.

It has to be mentioned that the phase synchronization bandwidth is mainly limited by the TE mode (see Figure 5), as the frequency dispersion behavior of this mode changes faster with frequency than the TM SW dispersion.

3.3. Metasurface Implementation Details

In this section, the implementation details of a SW-guiding MTS are given, in which two TM and TE modes are guided, decoupled and phase-balanced (Figure 6). Pixel B, presented in the previous Section 3.2, has been employed to implement a SW-guiding surface with a total radius of $R = 50u = 157$ mm $= 7\lambda_0$. At each position on the surface, the metallic elliptical patch is printed on top of the grounded dielectric, based on a cartesian lattice meshgrid (unit cell dimension $u = 3.14$ mm). Each patch is appropriately rotated, in such a way that the minor axis of the ellipse meets the impinging

angle of the SWs propagating from the center of the structure, i.e., is aligned with $\hat{\rho}$. The structure is excited by a magnetic dipole oriented towards the y-axis.

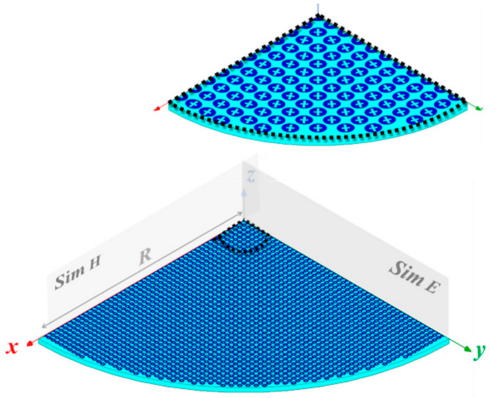

Figure 6. Details of the rotationally symmetric metasurface composed by pixel B subwavelength elements. Total radius $R = 50u = 157$ mm. The structure is excited by a magnetic dipole oriented towards the y-axis. The metal patches are shown in dark blue, whereas the light blue color represents the dielectric substrate.

4. Simulation Results

Employing appropriate symmetry conditions (see Figure 6), a quarter of the MTS structure was simulated using ANSYS HFSS software package. Two TM and TE modes are excited by a magnetic dipole oriented towards the y-axis. The total near-field components at 13.5 GHz obtained by the combination of both modes guided on the structure are depicted in Figure 7.

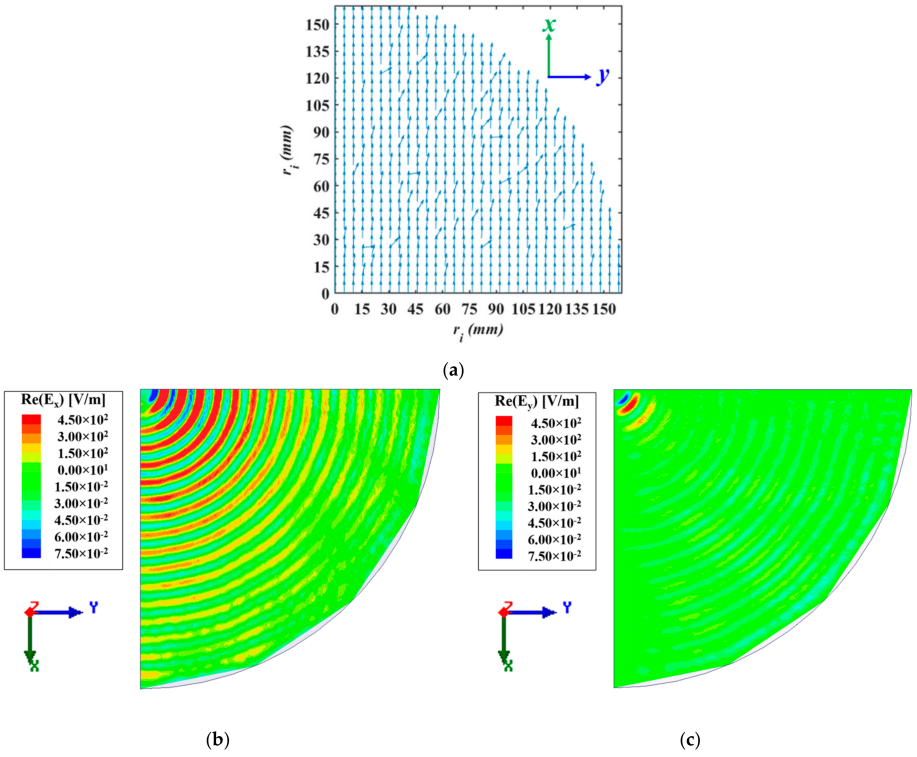

Figure 7. (**a**) Total field vector at 13.5 GHz over the MTS obtained as the combination of TM and TE modes; (**b**) $Re(E_x)$ and (**c**) $Re(E_y)$ components' magnitude over the surface.

The TM and TE modes were appropriately excited on the structure, with propagation that was synchronized and in-phase. Due to this fact, the TM and TE modes' field combination generates a total field oriented towards the *x*-axis (Figure 7a). Additionally, the decoupled propagation of both modes ensures negligible cross polar field excitation. In consequence, $Re(E_y)$ is negligible in Figure 7c.

Figure 8 depicts the total $Re(E_x)$ field in the aperture at φ = 0°, 45° and 90° planes, obtained as a combination of the synchronized TM and TE SW fields.

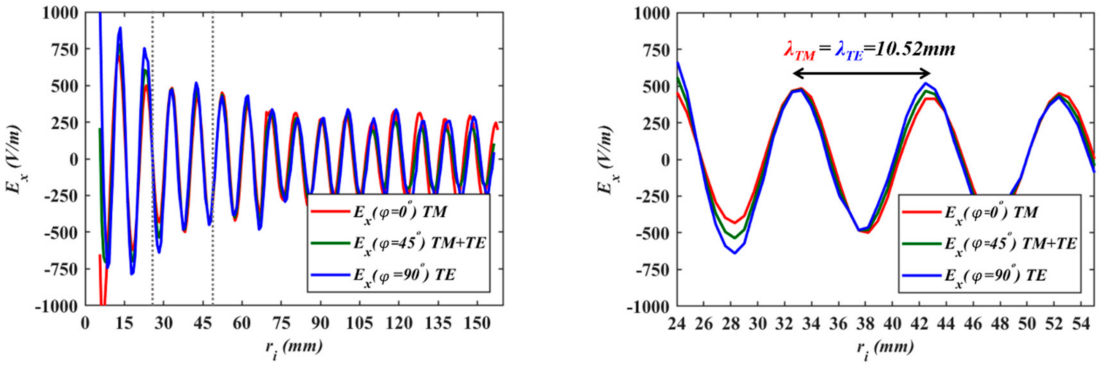

(**a**) (**b**)

Figure 8. (**a**) *Re(E_x)* field in the aperture ($R = 50u = 157$ mm) at $\varphi = 0°, 45°, 90°$ as a combination of the TM and TE SW fields; (**b**) Zoom of the curves.

As expected, the SW wavelengths of both modes are in agreement, $\lambda_{TM} = \lambda_{TE} = 10.52$ mm (Figure 8b). This feature is in agreement with the predicted phase velocity values related to the unit cell dispersion analysis carried out in Section 3.2, where $\beta_{TM} = \beta_{TE} = 597$ rad/m. It has to be noted that the synchronism of both modes is perfectly maintained in the center of the antenna. Nevertheless, for the outer positions ($r_i > 5.5\lambda_0$), there is some phase difference between the modes. The reason for this effect may be related to the cartesian lattice for the surface implementation, and its effect on the TE dispersion properties when the patch is rotated azimuthally.

5. Conclusions

Design details of a single-layer rotationally symmetric metasurface ensuring decoupled and synchronized propagation of TM and TE modes has been presented in this work. The MTS was implemented by means of a dense layer of subwavelength metallic elliptical patches with an asymmetric cross-shaped aperture in the center, printed on top of a grounded dielectric. With such a pixel geometry, the dispersion properties of TM and TE SWs match at the working frequency (13.5 GHz), and the total field generated on the aperture by the combination of both modes is perfectly linearly polarized. The design of such structures has important applications in the development of dual circularized polarized MTS antennas based on surface impedance modulation, in which TM and TE mode propagation with similar dispersion properties is required.

Acknowledgments: The authors would like to thank the financial support by the Spanish Ministry of Economy and Competitiveness, Project No. TEC2013-47753-C3-1-R and TEC2016-76997-C3-1-R and by the Gobierno de Navarra, Project PI017 COMUNICACIONES 5G and PI018 COMUNICACIONES 5G.

Author Contributions: Amagoia Tellechae and Juan Carlos Iriarte conceived and designed the experiments; Amagoia Tellechea performed the experiments; Iñigo Ederra y Ramón Gonzalo analyzed the data; Amagoia Tellechea, Iñigo Ederra y Juan Carlos Iriarte wrote the paper.

Conflicts of Interest: The authors declare no conflict of interest.

References

1. Fong, B.H.; Colburn, J.S.; Ottusch, J.J.; Visher, J.L.; Sievenpiper, D.F. Scalar and tensor holographic artificial impedance surfaces. *IEEE Trans. Antennas Propag.* **2010**, *58*, 3212–3221. [CrossRef]
2. Bilow, H.J. Guided waves on a planar tensor impedance surface. *IEEE Trans. Antennas Propag.* **2003**, *51*, 2788–2792. [CrossRef]
3. Sievenpiper, D.; Colburn, J.; Fong, B.; Ottusch, J.; Visher, J. Holographic artificial impedance surfaces for conformal antennas. In Proceedings of the 2005 IEEE Antennas and Propagation Society International Symposium, Washington, DC, USA, 3–8 July 2005.
4. Jiang, L.; Grbic, A.; Merlin, A. Near-field plates: Subdiffraction focusing with patterned surfaces. *Science* **2008**, *320*, 511–513.
5. Pfeiffer, P.; Grbic, A. Planar lens antennas of subwavelength thickness: Collimating leaky-waves with metasurfaces. *IEEE Trans. Antennas Propag.* **2015**, *63*, 3248–3253. [CrossRef]
6. Martini, E.; Mencagli, M.; Maci, S. Metasurface transformation for surface wave control. *Philos. Trans. R. Soc. A* **2015**, 373. [CrossRef] [PubMed]
7. González-Ovejero, D.; Martini, E.; Maci, S. Surface waves supported by metasurfaces with self-complementary geometries. *IEEE Trans. Antennas Propag.* **2015**, *63*, 250–260. [CrossRef]
8. Patel, A.M.; Grbic, A. Modeling and analysis of printed-circuit tensor impedance surfaces. *IEEE Trans. Antennas Propag.* **2013**, *61*, 211–220. [CrossRef]
9. Mencagli, M.; Martini, E.; Maci, S. Surface wave dispersion for anisotropic metasurfaces constituted by elliptical patches. *IEEE Trans. Antennas Propag.* **2015**, *63*, 2992–3003. [CrossRef]
10. Granet, G.; Luukkonen, O.; Simovski, C.; Tretyakov, S.A. Simple and accurate analytical model of planar grids and high-impedance surfaces comprising metal strips or patches. *IEEE Trans. Antennas Propag.* **2008**, *56*, 1624–1632.
11. Mencagli, M.; Martini, E.; Maci, S. Transition function for closed-form representation of metasurface reactance. *IEEE Trans. Antennas Propag.* **2016**, *64*, 136–145. [CrossRef]
12. Mencagli, M.; Giovampaola, C.D.; Maci, S. A closed-form representation of isofrequency dispersion curve and group velocity for surface waves supported by anisotropic and spatially dispersive metasurfaces. *IEEE Trans. Antennas Propag.* **2016**, *64*, 2319–2327. [CrossRef]
13. Oliner, A.; Hessel, A. Guided waves on sinusoidally-modulated reactance surfaces. *IRE Trans. Antennas Propag.* **1959**, *7*, 201–208. [CrossRef]
14. Minatti, G.; Maci, S.; De Vita, P.; Freni, A.; Sabbadini, M. A circularly-polarized isoflux antenna based on anisotropic metasurface. *IEEE Trans. Antennas Propag.* **2012**, *60*, 4998–5009. [CrossRef]
15. Minatti, G.; Faenzi, M.; Martini, E.; Caminita, F.; De Vita, P.; González-Ovejero, D.; Sabbadini, M.; Maci, S. Modulated metasurface antennas for space: Synthesis, analysis and realizations. *IEEE Trans. Antennas Propag.* **2015**, *63*, 1288–1300. [CrossRef]
16. Minatti, G.; Caminita, F.; Casaletti, M.; Maci, S. Spiral leaky-wave antennas based on modulated surface impedance. *IEEE Trans. Antennas Propag.* **2011**, *59*, 4436–4444. [CrossRef]
17. Faenzi, M.; Caminita, F.; Martini, E.; de Vita, P.; Minatti, G.; Sabbadini, M.; Maci, S. Realization and measurement of broadside beam modulated metasurface antennas. *IEEE Antennas Wirel. Propag. Lett.* **2016**, *15*, 610–613. [CrossRef]
18. Gonzalez-Ovejero, D.; Minatti, G.; Chattopadhyay, G.; Maci, S. Multibeam by metasurface antennas. *IEEE Trans. Antennas Propag.* **2017**, *65*, 2923–2930. [CrossRef]
19. Tellechea, A.; Caminita, F.; Martini, E.; Ederra, I.; Iriarte, J.C.; Gonzalo, R.; Maci, S. Dual circularly polarized broadside beam metasurface antenna. *IEEE Trans. Antennas Propag.* **2016**, *64*, 2944–2953. [CrossRef]
20. Tellechea, A.; Iriarte, J.C.; Ederra, I.; Gonzalo, R.; Martini, E.; Maci, S. Experimental validation of a Ku-band dual circularly polarized metasurface antenna. *IEEE Trans. Antennas Propag.* **2018**, *66*, 1153–1159.